electronics

MDPI

Article

Dual-Channel Secure Communication Based on Wideband Optical Chaos in Semiconductor Lasers Subject to Intensity Modulation Optical Injection

Youming Wang [1,2], Yu Huang [1,2], Pei Zhou [1,2,*] and Nianqiang Li [1,2,*]

[1] School of Optoelectronic Science and Engineering & Collaborative Innovation Center of Suzhou Nano Science and Technology, Soochow University, Suzhou 215006, China
[2] Key Lab of Advanced Optical Manufacturing Technologies of Jiangsu Province & Key Lab of Modern Optical Technologies of Education Ministry of China, Soochow University, Suzhou 215006, China
* Correspondence: peizhou@suda.edu.cn (P.Z.); wan_103301@163.com (N.L.)

Abstract: Chaotic optical communication was initially proposed to provide advanced physical layer security for optical communication. Here, we propose and numerically demonstrate an optical chaos communication scheme based on semiconductor lasers subject to intensity modulation optical injection for secure transmission of quadrature amplitude modulation (QAM) messages. In this scheme, two chaotic sources were generated with different modulation parameters and acted as chaotic carriers at the transmitter side, which were subsequently used to drive two receivers in two separate channels. Numerical results demonstrate that this scheme allows for broadband chaos generation and high-quality chaos synchronization can be achieved to simultaneously encrypt two messages for secure communication; a 20 GBaud 16-QAM message was recovered correctly with a transmission distance in standard single mode fiber (SMF) over 120-km, while the other 20 GBaud 64-QAM message was limited to a 20-km fiber transmission distance. The system performance was systematically evaluated by analyzing the bit error ratio (BER) of the recovered message versus the masking coefficient and the transmission distance. Furthermore, our simulations justify the robustness against the mismatch of parameters. Therefore, we hope that this scheme can be experimentally implemented for high-speed chaos communication and secure key distribution.

Keywords: intensity modulation; bandwidth; chaos synchronization; secure communication

Citation: Wang, Y.; Huang, Y.; Zhou, P.; Li, N. Dual-Channel Secure Communication Based on Wideband Optical Chaos in Semiconductor Lasers Subject to Intensity Modulation Optical Injection. *Electronics* **2023**, *12*, 509. https://doi.org/10.3390/electronics12030509

Academic Editors: Elias Stathatos and Paulo Monteiro

Received: 13 December 2022
Revised: 31 December 2022
Accepted: 14 January 2023
Published: 18 January 2023

1. Introduction

Chaotic optical communication as a kind of physical layer encryption technology has been widely studied due to the large bandwidth and noise-like properties of optical chaos [1–6]. Very recently, it has also been applied to mid-infrared free-space secure communication by virtue of two unidirectionally coupled quantum cascade lasers at a wavelength of 5.7 μm [7]. The external-cavity semiconductor laser (ECL), e.g., the laser with all-optical feedback [8], optoelectronic feedback [9], or electro-optic feedback [10], is a common scheme to generate an optical chaos source because of its simple structure and rich dynamics. However, it has been demonstrated that some key parameters of the ECL system, i.e., the bias current [11], external-cavity length [12], and feedback strength [13], cannot be the safe key for secure chaos communication. For example, as a result of the periodic modulation pattern induced by external cavity resonance, an obvious time-delay signature (TDS) will appear when computing, e.g., the auto-correlation properties of chaotic intensity time series. The TDS is a threat to communication security due to its risk of information leakage of the time delay, i.e., the external-cavity length.

To solve this problem, many TDS suppression schemes have been proposed, including chaotic self-phase-modulation [14], dual optical feedback [15–17], fiber Bragg grating

(FBG) feedback [18,19], and optical or electronic heterodyning [20,21]. Although the aforementioned schemes provide promising methods for the concealment of TDS, it inevitably increases the complexity of the system. Alternatively, continuous wave (CW) optical injection in semiconductor lasers system has been proposed to generate optical chaos because it is easy to implement and does not introduce TDS [22–24]. For example, Lin et al. experimentally demonstrated that a semiconductor laser subjected to CW injection can produce a chaos signal without TDS [25]. Although the TDS is not introduced into this scheme, optical chaos can only be found in the limited parameter space as the frequency detuning versus the optical injection level is varied [26]. Additionally, the relatively narrow chaotic bandwidth of this scheme is unsatisfactory for chaos-based applications. Therefore, it is very important and interesting to explore a simple structure to improve the bandwidth and generate the required optical chaos source in the wide range of parameters. To this end, modulation optical injection has been proposed to improve the chaotic bandwidth and the size of the chaotic region. Chan et al. numerically demonstrated that a semiconductor laser subject to intensity modulation (IM) optical injection can generate optical chaos with a bandwidth of about 22 GHz at a larger modulation depth [27]. Nevertheless, such a modulation depth results in the emergence of narrow peaks in the power spectrum, which is inappropriate for chaos-based applications. Fortunately, Tseng et al. optimized the scheme, selecting the modulation frequency of a few GHz of modulation frequency away from the lower oscillation sideband of the period-one dynamic and the strong narrow peak can be effectively eliminated [28]. Afterwards, based on the revised IM scheme, Zeng et al. systematically and numerically analyzed the characteristics of chaotic signals and identified the region for high-quality chaos generation [29]. Recently, such high-quality chaos signals have attracted much research interest for technological application. For example, chaos with a broad bandwidth of 33 GHz was prepared and investigated for application in random number generation by Tseng et al. [30]. These results have shown that such a chaotic source can be applied as a 2-bit physical random number generator at a rate of 160 Gbit/s. For these reasons, it would be of interest to explore the possibility and performance of achieving high-speed chaotic optical communications based on such wideband chaos generated by the IM optical injection system.

In this paper, we propose and numerically demonstrate a novel chaotic optical communication scheme based on a master–slave configuration, where semiconductor lasers with IM optical injection are used as the chaotic sources. Specifically, we firstly prepared two independent optical chaos outputs with broad bandwidth by selecting different modulation parameters. Next, two symmetrical configurations were constructed to investigate the achievement conditions and properties of injection-locking chaos synchronization. Then, the generated wideband chaos outputs were used as optical carriers to encrypt two different messages and were injected into lasers at the receiver side through SMF. Finally, the capability of information recovery and constellation performance were investigated. The results indicate that high-speed chaotic secure communication with a good BER property and satisfactory mismatch robustness can be achieved.

2. Principles and Theoretical Model

The configuration of a dual-channel chaos communication system with IM optical injection is illustrated in Figure 1. A single-mode distributed feedback (DFB) semiconductor laser is deployed as a master laser (ML), and its output is injected into two twin single-mode DFB lasers—namely transmitter laser 1 (TL1) and transmitter laser 2 (TL2)—after passing through two Mach–Zehnder modulators (MZM) and two variable optical attenuators (VOA). The outputs of two transmitter lasers pass through two other MZMs. MZM3 is driven by a 16 quadrature amplitude modulation (16-QAM) message (Message 1) and MZM4 is driven by a 64 quadrature amplitude modulation (64-QAM) message (Message 2). Before being sent into the fiber link, the two outputs are amplified by the erbium doped fiber amplifier (EDFA). At the receiver side, the encrypted signal is split into two parts. One part is sent into a photodetector (PD1). Meanwhile, the other part is injected into the

receiver laser (RL1) to generate a reference signal and then it is sent into a photodetector (PD2). Message 1 can be decrypted by comparing the difference between the outputs of PD1 and PD2. Likewise, Message 2 can be extracted with the same method.

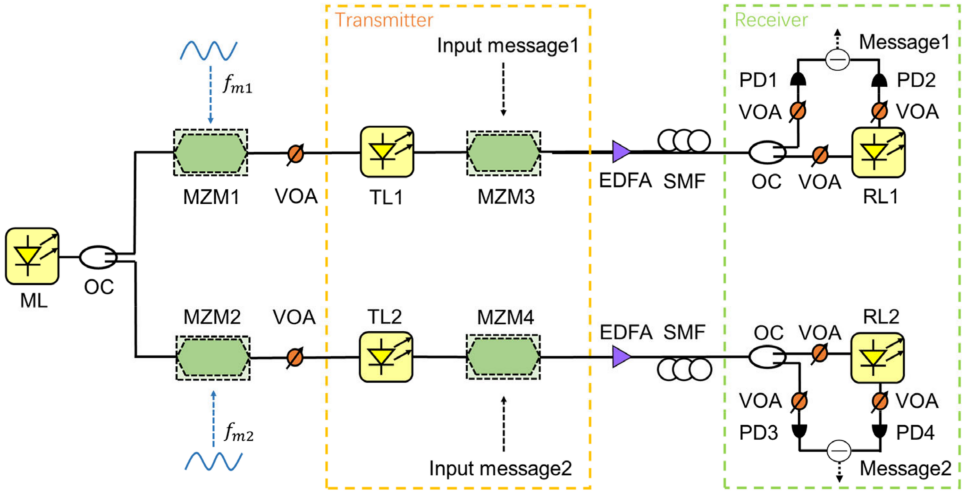

Figure 1. Schematic of dual-channel chaotic communication system subject to IM optical injection. ML, master laser; TL, transmitter lasers; RL, receiver lasers; MZM, Mach–Zehnder modulators; OC, optical coupler; VOA, variable optical attenuators; EDFA, erbium doped fiber amplifier; PD, photodetector.

For the numerical purpose, the proposed laser system can be modeled by the following rate equations [29,31]:

$$\begin{aligned}\frac{dE_{T_{1,2}}(t)}{dt} &= \tfrac{1}{2}(1+i\Gamma)\left\{G_n\left[N_{T_{1,2}}(t)-N_0\right]-\tfrac{1}{\tau_p}\right\}E_{T_{1,2}}(t)\\ &+\xi_i\left\{1+\left[m_{1,2}\exp(-i2\pi f_{m_{1,2}}t)+m_{1,2}\exp(i2\pi f_{m_{1,2}}t)\right\}\exp(2\pi f_i t)\right.\end{aligned} \tag{1}$$

$$\frac{dE_{R_{1,2}}(t)}{dt} = \frac{1}{2}(1+i\Gamma)\left\{G_n\left[N_{R_{1,2}}(t)-N_0\right]-\frac{1}{\tau_p}\right\}E_{R_{1,2}}(t)+k_{inj}E_{ext}(t) \tag{2}$$

$$\frac{dN_{T_{1,2},R_{1,2}}(t)}{dt} = \frac{I}{qV}-\frac{1}{\tau_n}N_{T_{1,2},R_{1,2}}(t)-G_n\left[N_{T_{1,2},R_{1,2}}(t)-N_0\right]\left|E_{T_{1,2},R_{1,2}}(t)\right|^2, \tag{3}$$

where the subscripts $T_{1,2}$, and $R_{1,2}$ stand for TL1, TL2, RL1 and RL2, respectively. $E(t)$ denotes the slowly varying complex amplitude of the electric field, and $N(t)$ represents the carrier density in the laser cavity. The other parameters are defined as follows: Γ is the linewidth enhancement factor, G_n is the gain coefficient, N_0 is the carrier density at transparency, τ_p is the photon lifetime, τ_n is the carrier lifetime, $I = 1.8I_{th}$ is the injection current (I_{th} is the threshold current), q is the electronic charge, and V is the volume of the active region. The output of the ML can be controlled by two injection parameters, i.e., ξ_i and f_i. The ξ_i is the injection ratio, which is described as the square root of the ratio of power between the optical injection signal and the free-running ML. The f_i is the frequency detuning, which represents the frequency offset of the injection from the free-running frequency of the ML, and f_i is defined by $f_i = \omega_i/2\pi$, where ω_i denotes the angular frequency offset. When the optical input of the TL is modulated by the MZM1 and the MZM2, the injection strength is defined as $\xi_i(1+(mexp(-i2\pi f_m t)+mexp(i2\pi f_m t)))$, where m is the modulation depth and f_m is the modulation frequency. The term $k_{inj}E_{ext}(t)$ in (2) is the external-injection field amplitude from the transmitter to the receiver which indicates the unidirectional coupling. k_{inj} is written as $k_{inj} = 1/\tau_{in}(1-r_0^2)r_{inj}/r_0$, where τ_{in} is the round-trip time in the laser cavity, r_0 is the amplitude reflectivity of the laser facet, and r_{inj} represents the amplitude reflectivity of the external mirror. At the transmitter, a

16-QAM message and a 64-QAM message are modulated on to the chaotic carrier through the MZM3 and the MZM4, respectively. Note here that the output of the MZM3/MZM4, i.e., the modulated signal, is given by $E_T(t)\cos\left(k_{MZM}M_{QAM(t)}+\varphi\right)$, where $E_T(t)$ represents the wideband chaotic signal generated from TL1 and TL2 by solving Equations (1)–(3); $M_{QAM(t)}$ are those two QAM messages, k_{MZM} is the message modulation depth and φ is the normalized bias of the MZM.

The fiber channels are described in terms of the nonlinear Schrödinger equation (NLSE) as [32]:

$$j\frac{\partial E}{\partial Z}=-\frac{1}{2}\alpha E+\frac{1}{2}\beta_2\frac{\partial^2 E}{\partial T^2}-\gamma|E|^2E, \tag{4}$$

where E is the slowly varying complex amplitude of the optical field, Z is the direction of propagation, and T is the time. For SMF, $\alpha=0.2$ dB/km is the attenuation coefficient, $\beta_2=-0.1$ ps^2/km is the dispersion coefficient, and $\gamma=1.5$ mW^{-1}km^{-1} is the nonlinear coefficient. The distributed Fourier method was used to handle this equation.

To quantify the bandwidth and the chaos synchronization quality, the effective bandwidth and the synchronization coefficients were calculated, respectively. The effective bandwidth is defined as the part between the DC and the frequency where 80% of the energy is contained in the power spectrum, as those in [33,34]. The cross-correlation (CC) function is defined as [35,36]:

$$CC=\frac{\langle(I(t+\Delta t)-\langle I(t+\Delta t)\rangle)\cdot(I(t)-\langle I(t)\rangle)\rangle}{(\left\langle(I(t+\Delta t)-\langle I(t+\Delta t)\rangle)^2\right\rangle\cdot\left\langle(I(t)-\langle I(t)\rangle)^2\right\rangle)^{1/2}}, \tag{5}$$

where $I(t)=|E(t)|^2$ is the intensity time series, $I(t+\Delta t)$ contains the time shift Δt with respect to $I(t)$, and $\langle\cdot\rangle$ stands for the time averaging. In our simulation, we solved the rate equations with the fourth-order Runge–Kutta algorithm. We chose 0.1 ps as the integration step length and 50 ns as the duration time of series. The definitions and values of the symbols used in the simulation are shown in Table 1 [31].

Table 1. Parameter values used in the numerical simulation.

Symbol	Parameter	Value
Γ	linewidth enhancement factor	4.5
G_n	gain coefficient	10^{-12} m^3/s
N_0	carrier density at transparency	10^{24} m^{-3}
τ_p	photon lifetime	2 ps
τ_n	carrier lifetime	2 ns
I_{th}	threshold current	18 mA
q	electronic charge	1.602×10^{-19} C
V	volume of the active region	1.5×10^{-16} m^3
ξ_i	injection ratio	40 ns^{-1}
f_i	frequency detuning	−30 GHz
τ_{in}	round-trip time	9 ps
r_0	amplitude reflectivity of the laser facet	0.3
r_{inj}	amplitude reflectivity of external mirror	0.1
k_{MZM}	message modulation depth	0.08
φ	the normalized bias	0.785

3. Numerical Results and Discussion

3.1. Synchronization Characteristics of Wideband Chaos Signals

In this section, we first calculated the effective bandwidth and the synchronization coefficient. It was theoretically confirmed that wideband optical chaos can be generated under the effect of IM optical injection in our previous work [29]. In this simulation, we chose (m, f_m) = (0.11, 30 GHz) as those of the first channel and (m, f_m) = (0.26, 40 GHz) as the modulation parameters of the second channel. Figure 2 shows the time series, the

power spectra and the phase portraits of the optical chaotic signals generated by the IM optical injection. As can be seen, the temporal waveforms are aperiodic and noise-like, exhibiting the feature of chaos. Thanks to the strong injection locking, almost the same fluctuations between the transmitter and the receiver in both communication channels can be obtained; please compare Figure 2a,b and compare Figure 2e,f. On the contrary, the intensity oscillations between the two channels are almost completely different. The power spectra shown in Figure 2c,g were calculated from the time domain signal based on the fast Fourier transform (FFT) algorithm. Following the algorithm mentioned above, the effective bandwidth was estimated as 22.18 GHz and 25.46 GHz for Figure 2c,g, respectively, which confirms the generation of wideband chaos in our proposed scheme. The phase portraits plotted in Figure 2d,h also show the characteristics of the chaotic state, from which no discernible structure can be seen, from the complex attractor.

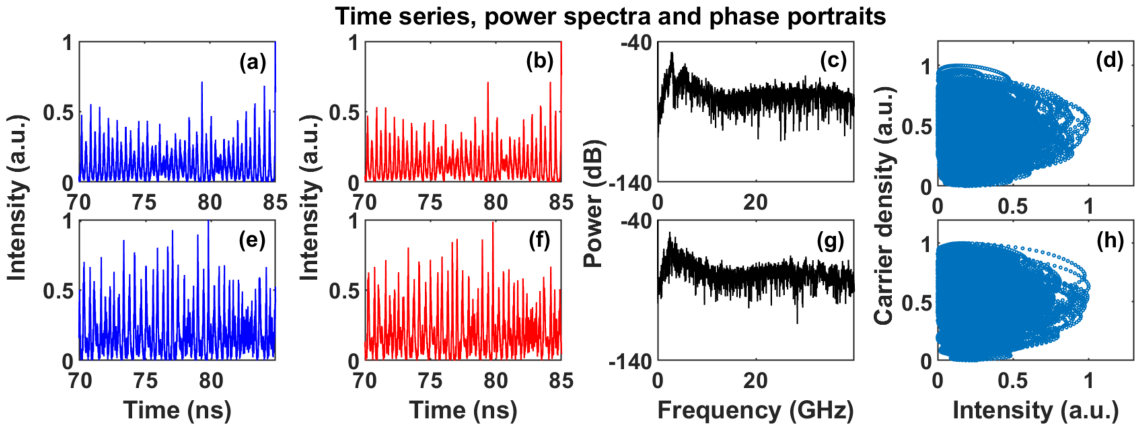

Figure 2. Time series of (**a**,**e**) the first channel and (**b**,**f**) the second channel of TLs and RLs. (**c**,**g**) Power spectra of TLs. (**d**,**h**) Phase portraits of TLs.

Figure 3 illustrates the synchronization performance of the optical chaotic signals. In the synchronization plot of Figure 3a,b, we observe that the whole dots are converged along the diagonal line of the panel. This means that high-quality chaos synchronization is realized between the transmitter and the receiver, where the maximal cross−correlation coefficient $CC_{max} = 0.982$ in the first channel and $CC_{max} = 0.956$ in the second channel. On the contrary, all the dots are divergent as shown in the synchronization plot of Figure 3c, where the CC_{max} value is calculated to be only 0.123 and it confirms that there is negligible synchronization achieved between the two chaotic sources. Thus, this system can support independent dual-channel secure communication to encrypt two different messages at the same time.

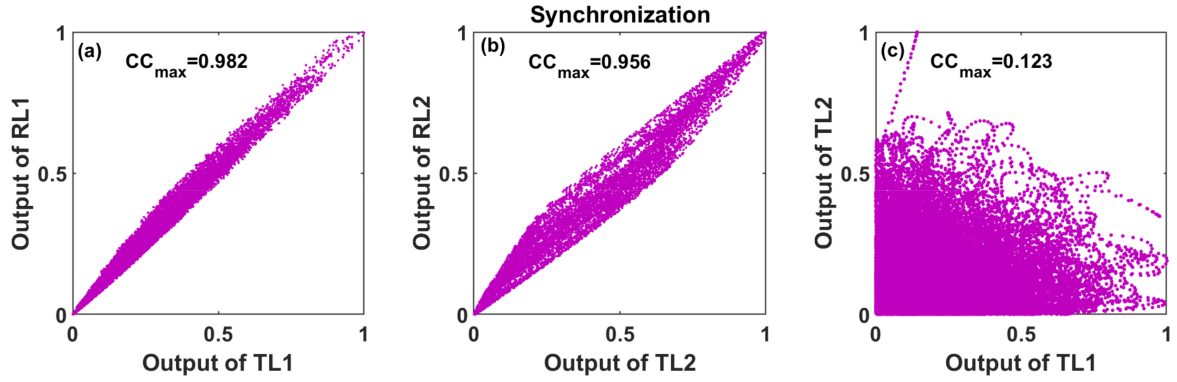

Figure 3. The synchronization plot between (**a**) TL1 and RL1, (**b**) TL2 and RL2, (**c**) TL1 and TL2.

3.2. Performance of Secure Communication

Next, we studied the application of the proposed wideband chaos signals in optical secure communication. To improve bandwidth utilization, we chose the modulation information combining amplitude and phase modulation methods instead of a conventional single binary sequence. In this simulation, Message 1 is a 16−QAM message and Message 2 is a 64-QAM message, respectively. Both QAM messages are modulated by random data after serial−to−parallel conversion, which is generated by the Mersenne Twister algorithm. The rate of the two messages is 20 GBaud, which indicates that Message 1 is equal to an 80 Gbit/s on−off keying (OOK) message and Message 2 is equal to a 120 Gbit/s OOK message, respectively. Figure 4 presents the performance of recovered messages under the back−to−back (BtB) transmission for Message 1 (first column) and Message 2 (second column). The original messages are shown by the red lines, while the recovered messages are depicted by the blue lines. Note that, as shown by the red lines of Figure 4, Gaussian noise was added into the original QAM messages to simulate the noise from modulators. At the receiver side, we can demodulate the message into two components: one is the quadrature component and the other is the in−phase component. In each component, the 16−QAM message has four levels and the 64−QAM message has eight levels. As can be seen in Figure 4, the successful decryption of the two QAM messages can be confirmed by comparing the level positions between original messages and recovered messages. It should be noted that the BER evaluation discussed below is also based on the comparison of the level positions of the original messages and the recovered messages.

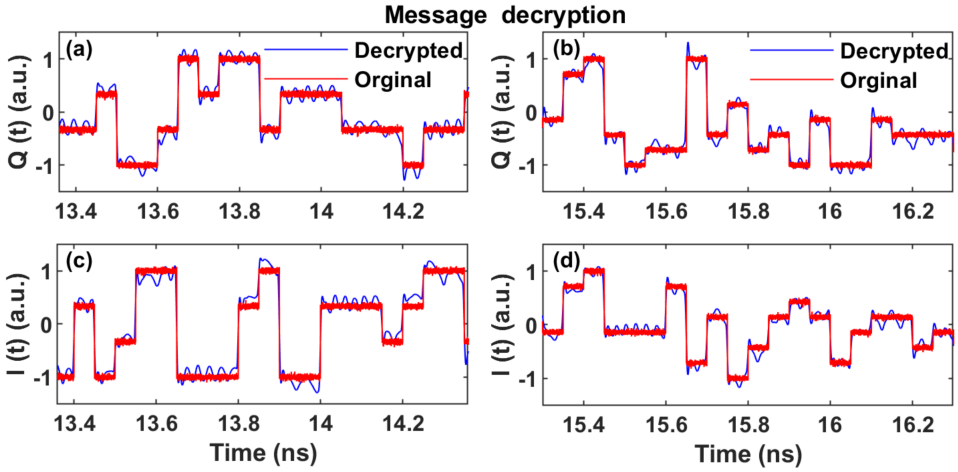

Figure 4. (**a**,**c**) Message 1 and (**b**,**d**) Message 2 of the original, decrypted (**a**,**b**) Q (t) signals and the original, decrypted (**c**,**d**) I (t) signals.

Then, the message transmission in the optical fiber was considered. Original messages are expressed as the red points, while the messages of legal decryption are the blue points and those intercepted by attack are the green points in the constellation of Figure 5. Compared with the decrypted 16−QAM message shown in Figure 5a,b, the decrypted 64−QAM message is worse under the same transmission distance, shown in Figure 5d,e. This is because the 64−QAM message has closer constellation points than the 16−QAM message. With the increase of various disturbances in the transmission link, the radius of partial constellation points becomes greater. When distances between some constellation points are shorter than their own radius, they will interfere with each other between symbols and the accuracy of message recovery will decrease sharply. Figure 5c,f show the recovered messages of a possible attack case called the direct detection with linear filtering (DDLF) attack [37]. In this kind of attack method, the eavesdropper directly detects the encrypted signal after chaotic masking and then sets the filter with a cut−off frequency equal to the bit rate of the signal to decipher information in the BtB situation. Obviously, regardless of

Message 1 or Message 2, the constellation points of attack overlap totally and cannot be distinguished as shown in Figure 5c,f.

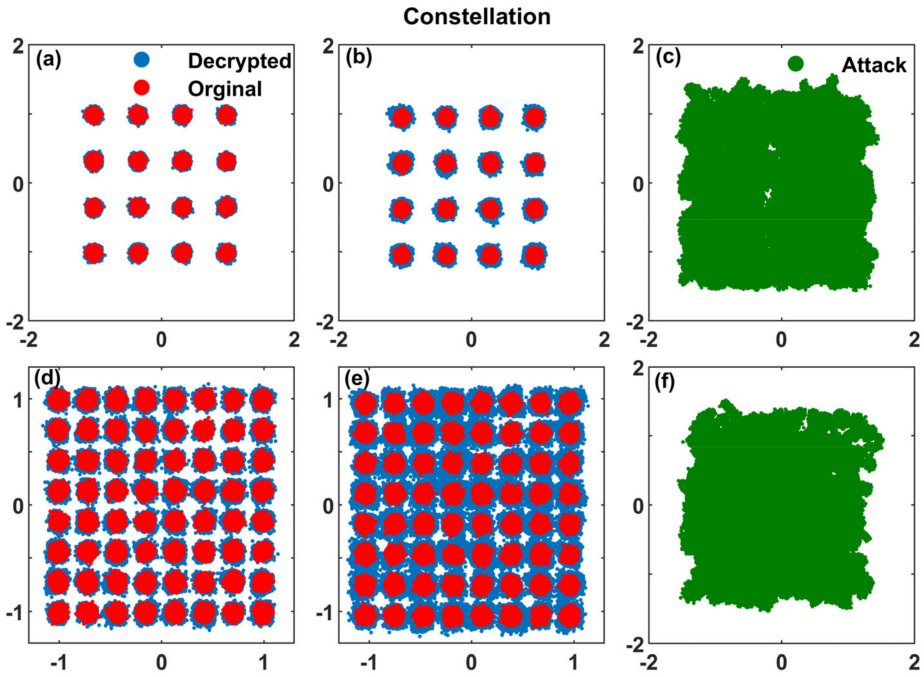

Figure 5. Constellations of the original, decrypted (**a**–**c**) Message 1 and (**d**–**f**) Message 2 transmission in (**a**,**d**) 10 km (first column), (**b**,**e**) 20 km (second column) optical fiber and (**c**,**f**) attack (third column).

We also studied the BER performance with different masking coefficients for the BtB case. The masking coefficient ρ is defined as the ratio of the peak value of the messages and the chaotic waveform. With the increase of the coefficient, the BER of the legal decryption and the attack decrease at the same time, shown in Figure 6. They intersect the hard decision forward error correction (HD−FEC) threshold line at points ρ_{min} and ρ_{max}, respectively. We regard $\Delta\rho = \rho_{max} - \rho_{min}$ as a valid masking coefficient range. The $\Delta\rho$ is 0.112 in Figure 6a and 0.259 in Figure 6b which means that Message 2 has a larger efficient range of the masking coefficient than Message 1. This result is explained as follows. For legal decryption, with the increase of modulation order, the bandwidth utilization will increase and more parts of chaotic signals need to encrypt information. It will further increase the remaining part of the chaotic synchronization signal after elimination, which is equivalent to reducing the signal−to−noise ratio. Therefore, this needs a larger amplitude of messages to decrypt correctly, and ρ_{min} will increase. For attack, the eavesdropper cannot cancel the chaotic carrier and the remaining part of the chaotic signal will increase more quickly. As a result, the growth rate of ρ_{max} is much faster than ρ_{min}, and then the $\Delta\rho$ becomes larger as the modulation order increases.

To further investigate the communication performance, we measured the BER of the recovered message for different transmission distances. As shown in Figure 7, the BER increases with the increase of transmission distance for both messages. We figured out that the maximum transmission distance of Message 1 reaches 120 km and that of Message 2 reaches 20 km by referring to the HD−FEC threshold (the dashed line in Figure 7). Like the phenomenon shown in Figure 5, the 16−QAM message can be transmitted to a longer distance in the SMF than the 64−QAM message. This is due to the fact that, as higher order information modulation formats have relatively closer symbol spacing, small differences brought by the continuous accumulation of the dispersion and nonlinearity in the optical fiber will lead to the misjudgment of symbols with the increase of the SMF length.

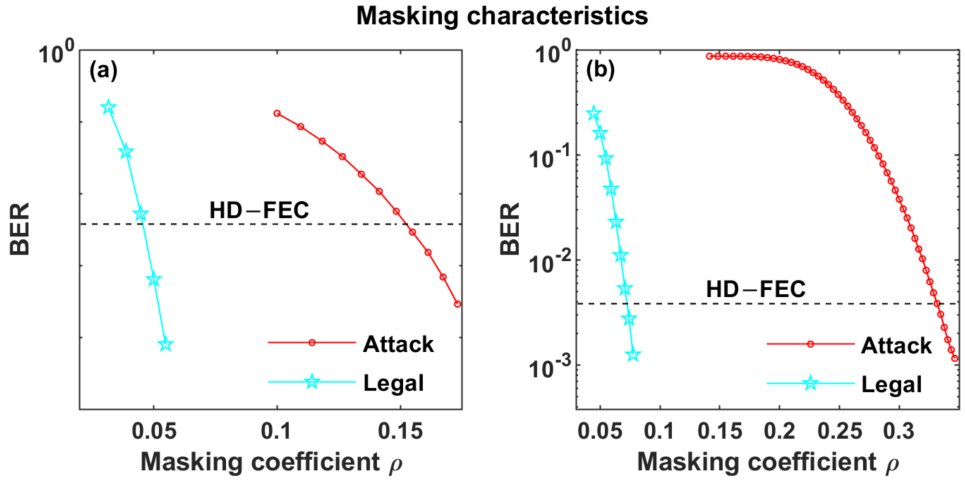

Figure 6. Masking characteristics of (**a**) Message 1 and (**b**) Message 2.

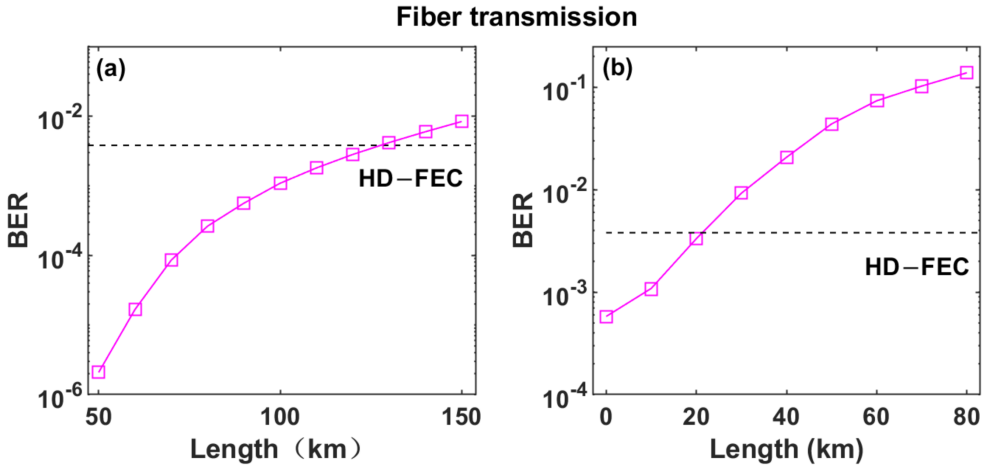

Figure 7. BER as a function of the fiber length for (**a**) Message 1 and (**b**) Message 2.

Under different degrees of the intrinsic parameter mismatch, Figure 8 finally presents the BER and the synchronization coefficient of Message 1 and Message 2 after transmitting over a distance in an optical fiber. We calculated the cross−correlation coefficient CC_{max} between the transmitter side and the receiver side to represent the synchronization performance. Here, mismatch is introduced according to the method reported in [38]: the parameters of the TLs are fixed, while those of the RLs are varied as follows, i.e., Γ, G_n and τ_n decreased, whereas τ_p and N_0 increased relatively by the same ratio. When the transmission distance of the two channels is close to their own longest distance, the results show that the trends of the communication capability versus the parameter mismatch are basically the same for both channels. The messages can be decrypted correctly with a satisfactory BER larger than the HD−FEC threshold in the mismatch range from −13% to 2%. Meanwhile, a high−quality injection−locking chaos synchronization between transmitters and receivers can be well maintained in this range, which is the prerequisite of the correct decryption.

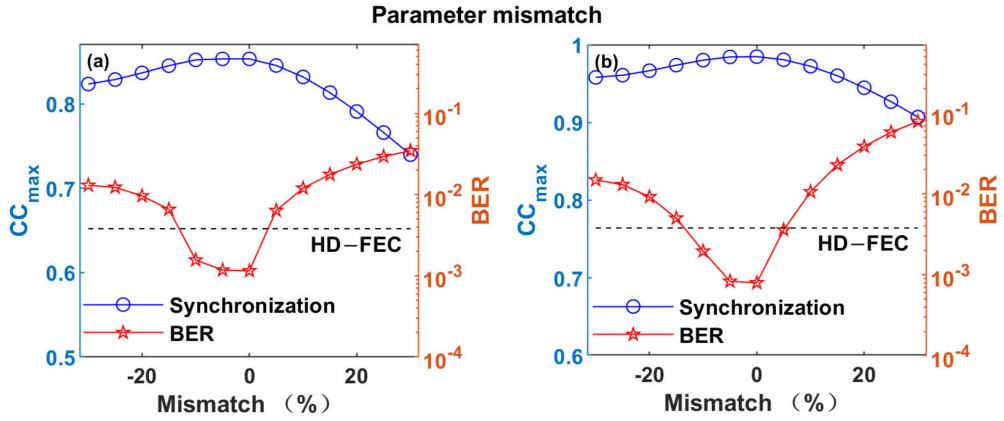

Figure 8. Parameter mismatch investigation for (**a**) Message 1 after 120 km transmission and (**b**) Message 2 after 20 km transmission.

4. Conclusions

In summary, we have proposed and numerically investigated the scheme for chaotic optical communication based on semiconductor lasers subject to IM optical injection. Two optical chaotic sources with effective bandwidth over 20 GHz were obtained and are almost independent by setting appropriate modulation parameters, which will be suitable for dual−channel secure communication. Moreover, the high−quality synchronization between the transmitter and receiver has been achieved by the injection−locking effect. The maximal synchronization coefficient has been calculated to be 0.982 in the first channel and 0.956 in the second channel, which enables the generated broadband chaotic carriers to encode and decode 16−QAM and 64−QAM messages for secure transmission. The investigation of the communication performance indicates that both messages with a baud rate of over 20 GBaud can be hidden within the chaos carriers successfully. The successful decryption at the legal receiver has been demonstrated after a 120 km transmission for the 16−QAM message and after a 20 km transmission for the 64−QAM in the SMF. We have also proved the encryption and robustness performance, which allows a satisfactory BER with a mismatch range from -13% to 2% in this scheme. Therefore, this study demonstrates that the wideband chaos generated by semiconductor lasers subject to IM optical injection can be applied to chaotic optical communication and can achieve some enhanced properties.

Author Contributions: Y.W., Y.H. and N.L. contributed to the idea and the writing of the manuscript. P.Z. and N.L. contributed to the reviewing and editing of the manuscript. All authors have read and agreed to the published version of the manuscript.

Funding: National Natural Science Foundation of China (62004135, 62001317, 62171305, 62111530301); Natural Science Research of Jiangsu Higher Education Institutions of China (20KJA416001); Natural Science Foundation of Jiangsu Province (BK20200855). The Open Fund of the State Key Laboratory of Millimeter Waves of China (K202239).

Data Availability Statement: Not applicable.

Conflicts of Interest: The authors declare no conflict of interest.

References

1. Van Wiggeren, G.D.; Roy, R. Communication with chaotic lasers. *Science* **1998**, *279*, 1198–1200. [CrossRef] [PubMed]
2. Argyris, A.; Syvridis, D.; Larger, L.; Annovazzi-Lodi, V.; Colet, P.; Fischer, I.; Garcia-Ojalvo, J.; Mirasso, C.R.; Pesquera, L.; Shore, K.A. Chaos-based communications at high bit rates using commercial fibre-optic links. *Nature* **2005**, *438*, 343–346. [CrossRef]
3. Lavrov, R.; Jacquot, M.; Larger, L. Nonlocal Nonlinear Electro-Optic Phase Dynamics Demonstrating 10 Gb/s Chaos Communications. *IEEE J. Quantum Electron.* **2010**, *46*, 1430–1435. [CrossRef]
4. Li, N.; Pan, W.; Yan, L.; Luo, B.; Xu, M.; Tang, Y.; Jiang, N.; Xiang, S.; Zhang, Q. Chaotic optical cryptographic communication using a three-semiconductor-laser scheme. *J. Opt. Soc. Am. B Opt. Phys.* **2012**, *29*, 101–108. [CrossRef]
5. Sciamanna, M.; Shore, K.A. Physics and applications of laser diode chaos. *Nat. Photonics* **2015**, *9*, 151–162. [CrossRef]

6. Jiang, N.; Zhao, A.; Xue, C.; Tang, J.; Qiu, K. Physical secure optical communication based on private chaotic spectral phase encryption/decryption. *Opt. Lett.* **2019**, *44*, 1536–1539. [CrossRef]
7. Spitz, O.; Herdt, A.; Wu, J.G.; Maisons, G.; Carras, M.; Wong, C.W.; Elsasser, W.; Grillot, F. Private communication with quantum cascade laser photonic chaos. *Nat. Commun.* **2021**, *12*, 1–8. [CrossRef]
8. Wang, A.; Wang, Y.; He, H. Enhancing the Bandwidth of the Optical Chaotic Signal Generated by a Semiconductor Laser With Optical Feedback. *IEEE Photonics Technol. Lett.* **2008**, *20*, 1633–1635. [CrossRef]
9. Li, M.; Hong, Y.; Wang, S.; Song, Y.; Sun, X. Radiation-induced mismatch effect on performances of space chaos laser communication systems. *Opt. Lett.* **2018**, *43*, 5134–5137. [CrossRef]
10. Li, N.; Susanto, H.; Cemlyn, B.; Henning, I.D.; Adams, M.J. Secure communication systems based on chaos in optically pumped spin-VCSELs. *Opt. Lett.* **2017**, *42*, 3494–3497. [CrossRef]
11. Wang, D.; Wang, L.; Li, P.; Zhao, T.; Jia, Z.; Gao, Z.; Guo, Y.; Wang, Y.; Wang, A. Bias Current of Semiconductor Laser: An Unsafe Key for Secure Chaos Communication. *Photonics* **2019**, *6*, 59. [CrossRef]
12. Zhao, Q.; Wang, Y.; Wang, A. Eavesdropping in chaotic optical communication using the feedback length of an external-cavity laser as a key. *Appl. Opt.* **2009**, *48*, 3515–3520. [CrossRef] [PubMed]
13. Li, N.; Pan, W.; Yan, L.; Luo, B.; Xu, M.; Jiang, N.; Tang, Y. On joint identification of the feedback parameters for hyperchaotic systems: An optimization-based approach. *Chaos Solitons Fractals* **2011**, *44*, 198–207. [CrossRef]
14. Kurdoglyan, M.S.; Kim, C.M.; Kim, G.U. Effects of nonlinear self-phase modulation of the transmitted signal on synchronization behavior of chaotic semiconductor lasers. *J. Opt. Soc. Am. B Opt. Phys.* **2004**, *21*, 2107–2111. [CrossRef]
15. Rontani, D.; Locquet, A.; Sciamanna, M.; Citrin, D.S. Loss of time-delay signature in the chaotic output of a semiconductor laser with optical feedback. *Opt. Lett.* **2007**, *32*, 2960–2962. [CrossRef] [PubMed]
16. Wang, L.; Wu, Z.-M.; Wu, J.-G.; Xia, G.-Q. Long-haul dual-channel bidirectional chaos communication based on polarization-resolved chaos synchronization between twin 1550 nM VCSELs subject to variable-polarization optical injection. *Opt. Commun.* **2015**, *334*, 214–221. [CrossRef]
17. Wu, J.-G.; Xia, G.-Q.; Wu, Z.-M. Suppression of time delay signatures of chaotic output in a semiconductor laser with double optical feedback. *Optics Express* **2009**, *17*, 20124–20133. [CrossRef] [PubMed]
18. Li, S.-S.; Liu, Q.; Chan, S.-C. Distributed Feedbacks for Time-Delay Signature Suppression of Chaos Generated From a Semiconductor Laser. *IEEE Photonics J.* **2012**, *4*, 1930–1935. [CrossRef]
19. Wang, L.; Mao, X.; Wang, A.; Wang, Y.; Gao, Z.; Li, S.; Yan, L. Scheme of coherent optical chaos communication. *Opt. Lett.* **2020**, *45*, 4762–4765. [CrossRef] [PubMed]
20. Cheng, C.-H.; Chen, Y.-C.; Lin, F.-Y. Chaos time delay signature suppression and bandwidth enhancement by electrical heterodyning. *Opt. Express* **2015**, *23*, 2308–2319. [CrossRef]
21. Wang, A.; Wang, L.; Li, P.; Wang, Y. Minimal-post-processing 320-Gbps true random bit generation using physical white chaos. *Opt. Express* **2017**, *25*, 3153–3164. [CrossRef]
22. Kovanis, V.; Gavrielides, A.; Simpson, T.B.; Liu, J.M. Instabilities and chaos in optically injected semiconductor-lasers. *Appl. Phys. Lett.* **1995**, *67*, 2780–2782. [CrossRef]
23. Wang, A.-B.; Wang, Y.-C.; Wang, J.-F. Route to broadband chaos in a chaotic laser diode subject to optical injection. *Opt. Lett.* **2009**, *34*, 1144–1146. [CrossRef]
24. Li, X.-Z.; Zhuang, J.-P.; Li, S.-S.; Gao, J.-B.; Chan, S.-C. Randomness evaluation for an optically injected chaotic semiconductor laser by attractor reconstruction. *Phys. Rev. E* **2016**, *94*, 042214. [CrossRef]
25. Lin, F.Y.; Liu, J.M. Chaotic lidar. *IEEE J. Sel. Top. Quantum Electron.* **2004**, *10*, 991–997. [CrossRef]
26. Hwang, S.K.; Liu, J.M. Dynamical characteristics of an optically injected semiconductor laser. *Opt. Commun.* **2000**, *183*, 195–205. [CrossRef]
27. Chan, S.-C.; Tang, W.K.S. Chaotic dynamics of laser diodes with strongly modulated optical injection. *Int. J. Bifurc. Chaos* **2009**, *19*, 3417–3424. [CrossRef]
28. Tseng, C.-H.; Hwang, S.-K. Broadband chaotic microwave generation through destabilization of period-one nonlinear dynamics in semiconductor lasers for radar applications. *Opt. Lett.* **2020**, *45*, 3777–3780. [CrossRef]
29. Zeng, Y.; Zhou, P.; Huang, Y.; Li, N. Optical chaos generated in semiconductor lasers with intensity-modulated optical injection: A numerical study. *Appl. Opt.* **2021**, *60*, 7963–7972. [CrossRef]
30. Tseng, C.-H.; Funabashi, R.; Kanno, K.; Uchida, A.; Wei, C.-C.; Hwang, S.-K. High-entropy chaos generation using semiconductor lasers subject to intensity-modulated optical injection for certified physical random number generation. *Opt. Lett.* **2021**, *46*, 3384–3387. [CrossRef] [PubMed]
31. Li, N.; Pan, W.; Luo, B.; Yan, L.; Zou, X.; Jiang, N.; Xiang, S. High Bit Rate Fiber-Optic Transmission Using a Four-Chaotic-Semiconductor-Laser Scheme. *IEEE Photonics Technol. Lett.* **2012**, *24*, 1072–1074. [CrossRef]
32. Mirasso, C.R.; Colet, P.; GarciaFernandez, P. Synchronization of chaotic semiconductor lasers: Application to encoded communications. *IEEE Photonics Technol. Lett.* **1996**, *8*, 299–301. [CrossRef]
33. Lin, F.Y.; Liu, J.M. Nonlinear dynamical characteristics of an optically injected semiconductor laser subject to optoelectronic feedback. *Opt. Commun.* **2003**, *221*, 173–180. [CrossRef]
34. Amiri, I.S.; Ali, J. Femtosecond Optical Quantum Memory Generation Using Optical Bright Soliton. *J. Comput. Theor. Nanosci.* **2014**, *11*, 1480–1485. [CrossRef]

35. Wang, A.; Yang, Y.; Wang, B.; Zhang, B.; Li, L.; Wang, Y. Generation of wideband chaos with suppressed time-delay signature by delayed self-interference. *Opt. Express* **2013**, *21*, 8701–8710. [CrossRef] [PubMed]
36. Li, N.; Pan, W.; Locquet, A.; Citrin, D.S. Time-delay concealment and complexity enhancement of an external-cavity laser through optical injection. *Opt. Lett.* **2015**, *40*, 4416–4419. [CrossRef] [PubMed]
37. Jiang, N.; Zhao, A.; Liu, S.; Xue, C.; Qiu, K. Chaos synchronization and communication in closed-loop semiconductor lasers subject to common chaotic phase-modulated feedback. *Opt. Express* **2018**, *26*, 32404–32416. [CrossRef]
38. Bogris, A.; Rizomiliotis, P.; Chlouverakis, K.E.; Argyris, A.; Syvridis, D. Feedback phase in optically generated chaos: A secret key for cryptographic applications. *IEEE J. Quantum Electron.* **2008**, *44*, 119–124. [CrossRef]